technische universität
dortmund

A new diffuse-interface model for step flow in epitaxial growth

Andreas Rätz

Preprint 2012-03 März 2012

Fakultät für Mathematik
Technische Universität Dortmund
Vogelpothsweg 87
44227 Dortmund

tu-dortmund.de/MathPreprints

A NEW DIFFUSE-INTERFACE MODEL FOR STEP FLOW IN EPITAXIAL GROWTH

ANDREAS RÄTZ

Abstract. In this work, we consider epitaxial growth of thin crystalline films. Thereby, we propose a new diffuse-interface approximation of a semi-continuous model resolving atomic distances in the growth direction but being coarse-grained in the lateral directions. Mathematically, this leads to a free boundary problem proposed by Burton, Cabrera and Frank for steps separating terraces of different atomic heights. The evolution of the steps is coupled to a diffusion equation for the adatom (adsorbed atom) concentration fulfilling Robin–type boundary conditions at the steps. Our approach allows to incorporate an Ehrlich–Schwoebel barrier as well as diffusion along step edges into a diffuse-interface model.

This model results in a Cahn–Hilliard equation with a degenerate mobility coupled to diffusion equations on the terraces with a diffuse-interface description of the boundary conditions at the steps. We provide a justification by matched asymptotic expansions formally showing the convergence of the diffuse-interface model towards the sharp-interface model as the interface width shrinks to zero. The results of the asymptotic analysis are numerically reproduced by a finite element discretisation.

1. Introduction

This work is concerned with thin film epitaxy, which is a technology of growing single crystals that inherit atomic structures from substrates. One example of thin film epitaxy is molecular beam epitaxy (MBE), where the deposition material is thermally evaporated from a source and forms a directed beam of atoms inside the chamber. Due to chemical bonding, atoms in the vapour are adsorbed by a given substrate or crystal surface.

We consider a microscopic picture of a stepped surface (see Fig. 1). Once adsorbed by the surface, the deposited atoms are called adatoms. Different mechanisms play a role such as adatom diffusion and desorption, deposition of atoms as well as attachment of adatoms from terraces to steps leading to a movement of steps, and detachment from steps to terraces. Furthermore, coalescence of a finite

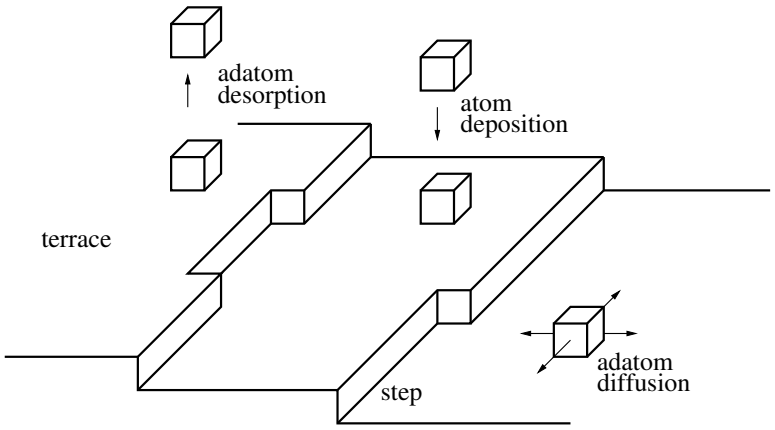

Figure 1. Microscopic processes on a stepped surface.

Date: March 16, 2012.

1991 *Mathematics Subject Classification.* Primary 35K35; Secondary 35K65; 65N30.

Key words and phrases. BCF–model; diffuse-interface; edge diffusion; attachment–detachment kinetics.

number of adatoms may lead to the nucleation of a new terrace or island and thus contribute to the growth of the film.

Burton, Cabrera and Frank [4] proposed a model ("BCF–model") for this situation. This step flow model is semi-continuous in the sense that it resolves atomic distances in the growth direction but is coarse-grained in the remaining directions (see e.g. [11, 15] for overviews on the BCF–model). In a mathematical description, steps are continuous curves separating terraces of different atomic heights. This leads to a free boundary problem similar to the Stefan problem modelling solidification processes. It includes a diffusion equation for an adatom concentration $\varrho : \Omega \times I \to \mathbb{R}$ with some domain $\Omega \subset \mathbb{R}^2$ and time interval $I = [0, T]$. The adatom concentration is then coupled to the movement of the steps whose normal velocities are mainly given by the sum of the adatom fluxes into the step from the upper and lower terraces, respectively and an additional term proportional to the second derivative with respect to arc length of the curvature of a step, modelling diffusion along step edges. On the boundaries, we assume in this work asymmetric Robin–type boundary conditions accounting for an asymmetry in attachment to upper and lower terraces, respectively. This is due to a higher energy barrier, the so-called Ehrlich–Schwoebel (ES) barrier (the denomination going back to [7, 23, 22]), that must be overcome by an adatom in order to attach from the upper terrace to a step. The asymmetry in attachment of adatoms to steps leads to morphological instabilities (see [2] for step trains and [12, 8] for circular islands). We emphasise that these boundary conditions lead to a jump in the adatom concentration at the steps, which makes a diffuse-interface description non-standard.

Phase-field approximations of the BCF–model with equilibrium boundary conditions at the steps have been proposed and numerically treated in [14, 10], with applications to one dimensional step trains and spiral growth, respectively. Diffuse-interface approximations for quasi-stationary BCF–type models including an ES barrier have been introduced in [19] and in [16], where an asymmetric degenerate mobility has been incorporated in a viscous Cahn–Hilliard equation accounting for the asymmetry in attachment to a step up or down, respectively. For a numerical treatment of this approach, we refer to [17, 25, 26]. A generalisation to anisotropic situations and its numerical discretisation can be found in [20]. Based on the treatment in [16], a generalisation including edge diffusion is proposed in [9] in a quasi-stationary situation and with an explicit treatment of edge diffusion in the numerical scheme.

In the present paper, we propose a new diffuse-interface approximation for the BCF–model including asymmetric boundary conditions and edge diffusion. Thereby, we combine the diffuse-interface approximation for motion by surface diffusion by a Cahn–Hilliard equation in [5] with the approach proposed in [13], where diffusion equations with different types of boundary conditions are treated in a diffuse-interface context. In this way, one can interpret the treatment presented here as diffuse-interface counterpart of the numerical sharp-interface treatment in [3]. One advantage of our model is that it incorporates the time derivative in the diffusion equation into a phase-field approximation for a BCF–model with asymmetric boundary conditions. Furthermore, it allows for an implicit numerical treatment of edge diffusion. Moreover, in [17] it is reported that in a numerical simulation of the model in [16] the steps are "behind" the analytic solution. This difficulty is not present in our approach.

In section 2, we give a brief description of the underlying sharp-interface model, i.e. the BCF–model. In section 3, we propose a diffuse-interface approximation for this model, and we provide a justification by matched asymptotic expansions, formally showing convergence towards the sharp-interface model as the width of the diffuse interface shrinks to zero. In addition, we discuss mass conservation and thermodynamical consistency. The results of the asymptotic analysis are numerically reproduced in section 4, where we compare numerical results with analytic solutions in one dimensional and rotationally symmetric two dimensional situations and with results of a stability analysis [12]. Furthermore, we apply the model to a case with more than two terraces to show the validity of the approach.

2. BCF–model

The mathematical description in the BCF-model includes a bounded domain $\Omega \subset \mathbb{R}^2$, which is given by projection of the film orthogonal to the growth direction. For simplicity, we start with considering

two terraces. This leads us to domains $\Omega_0, \Omega_1 \subset \Omega$ such that $\overline{\Omega} = \overline{\Omega}_0 \cup \overline{\Omega}_1$. Thereby, $\Omega_1 = \Omega_1(t)$ represents the upper terrace at time $t \in [0,T]$, which is of height one atomic layer higher than the lower terrace given by $\Omega_0 = \Omega_0(t)$. The position of the step $\Gamma(t) = \overline{\Omega_0(t)} \cap \overline{\Omega_1(t)}$, $t \in [0,T]$, is determined by the discrete height function $\varphi_0 : \Omega \times [0,T] \to \mathbb{R}$ at time t, $\varphi_0(\cdot,t) = \chi_{\Omega_1(t)}$ with the characteristic function $\chi_{\Omega_1(t)}$ of $\Omega_1(t)$. Furthermore, ν denotes the normal of Γ pointing from the upper terrace to the lower terrace (outer normal of Ω_1), and κ is the curvature of Γ. In addition, v denotes the normal velocity being positive for a growing upper terrace. The BCF–model then includes diffusion equations for the dimensionless adatom densities $\varrho_i : \overline{\Omega_i(t)} \times [0,T] \to \mathbb{R}$, $i = 0,1$,

$$\partial_t \varrho_i = D\Delta\varrho_i + F - \tau_d^{-1}\varrho_i \quad \text{in} \quad \Omega_i,\ i = 0,1. \tag{1}$$

Thereby, $D > 0$ is a dimensionless diffusion coefficient, F denotes a dimensionless deposition flux and τ_d^{-1} is a desorption rate. These are all assumed constant. At the step $\Gamma(t)$, we prescribe kinetic boundary conditions assuming that we have a balance between the adatom fluxes q_i, $i = 0,1$, on the left hand sides and the deviation from the thermodynamic equilibria on the right hand sides:

$$q_0 := D\nabla\varrho_0 \cdot \nu + v\varrho_0 = k_+(\varrho_0 - \varrho^*(1+\gamma\kappa)) \quad \text{(step up)}, \tag{2}$$

$$q_1 := -D\nabla\varrho_1 \cdot \nu - v\varrho_1 = k_-(\varrho_1 - \varrho^*(1+\gamma\kappa)) \quad \text{(step down)}. \tag{3}$$

Here, the constant ϱ^* is a dimensionless thermodynamic equilibrium of a straight step. By the constant γ we denote the step stiffness. The constants $k_\pm$ are the dimensionless attachment rates for attachment to a step up and down, respectively. The relation $k_+ > k_-$ thereby models the Ehrlich–Schwoebel barrier. The normal velocity of the step is given by

$$v = q_0 + q_1 + \beta\partial_s^2\kappa, \tag{4}$$

where the dimensionless constant β is related to the mobility of an edge atom along a curved step [11]. In order to obtain a well defined second derivative of the curvature, we assume C^4–regularity for $\Gamma(t)$, $t \in [0,T]$. Moreover, we suppose initial conditions

$$\varrho_i(x,0) = \hat{\varrho}_i(x) \quad \text{for} \quad x \in \overline{\Omega_i(0)},\ i = 0,1, \quad \text{and} \quad \Gamma(0) = \hat{\Gamma}$$

for given functions $\hat{\varrho}_i : \overline{\Omega_i(0)} \to \mathbb{R}$, $i = 0,1$, and steps $\hat{\Gamma}$ as well as boundary conditions for the densities

$$\nabla\varrho_i \cdot \nu_{\partial\Omega} = 0 \quad \text{on} \quad \partial\Omega \cap \overline{\Omega}_i,\ i = 0,1,$$

where $\nu_{\partial\Omega}$ is the outer normal to $\partial\Omega$.

3. Diffuse-interface approximation

We propose a diffuse-interface approximation of the above BCF–model. Thereby, the discrete height function φ_0 is smeared out on a length scale $O(\varepsilon)$ with a small parameter $\varepsilon > 0$, which yields the phase-field function (or smeared out height function) $\varphi : \Omega \times [0,T] \to \mathbb{R}$. We combine the approaches in [5] and in [13], in order to couple diffusion equations in Ω_0 and Ω_1 to the evolution of the steps based on edge diffusion and adatom fluxes in a diffuse-interface description. To be more precise, we consider in $\Omega \times [0,T]$ the system

$$\begin{aligned}\partial_t((1-\varphi)\varrho_0) = {} & D\nabla\cdot((1-\varphi)\nabla\varrho_0) + (1-\varphi)F - (1-\varphi)\tau_d^{-1}\varrho_0 \\ & - \varepsilon^{-1}B(\varphi)k_+(\varrho_0 - \varrho^*(1+\gamma\mu)),\end{aligned} \tag{5}$$

$$\partial_t(\varphi\varrho_1) = D\nabla\cdot(\varphi\nabla\varrho_1) + \varphi F - \varphi\tau_d^{-1}\varrho_0 - \varepsilon^{-1}B(\varphi)k_-(\varrho_1 - \varrho^*(1+\gamma\mu)), \tag{6}$$

$$\begin{aligned}\partial_t\varphi = {} & \varepsilon^{-1}\beta\nabla\cdot(B(\varphi)\nabla\mu) + \varepsilon^{-1}B(\varphi)(k_+(\varrho_0 - \varrho^*(1+\gamma\mu)) \\ & + k_-(\varrho_1 - \varrho^*(1+\gamma\mu))),\end{aligned} \tag{7}$$

$$\mu = -\varepsilon\Delta\varphi + \varepsilon^{-1}G'(\varphi). \tag{8}$$

Thereby, we use a normalised double well potential

$$G(\varphi) := 18\varphi^2(1-\varphi)^2. \tag{9}$$

Note that this choice of G guarantees

$$\int_0^1 \sqrt{2G(\varphi)}\,\mathrm{d}\varphi = 1.$$

Furthermore, we use the restricting function $B(\varphi) := 2G(\varphi)$. The variable μ in (8) is the functional derivative of a Ginzburg–Landau energy

$$\mathcal{E}(\varphi) := \int_\Omega \Big(\frac{\varepsilon}{2}|\nabla\varphi|^2 + \varepsilon^{-1}G(\varphi)\Big)\,\mathrm{d}x,$$

which is a diffuse-interface approximation of the total length of the steps. Therefore, μ is a diffuse-interface counterpart of the curvature of the steps.

We assume initial conditions

$$\varrho_i(x,0) = \hat{\varrho}_i(x),\ i = 0,1, \quad \varphi(x,0) = \hat{\varphi}_0(x) \quad \text{for} \quad x \in \overline{\Omega},$$

for given functions $\hat{\varphi}$, $\hat{\varrho}_i : \overline{\Omega} \to \mathbb{R}$, $i = 0,1$ and boundary conditions

$$\nabla\varrho_0 \cdot \nu_{\partial\Omega} = \nabla\varrho_1 \cdot \nu_{\partial\Omega} = \nabla\varphi \cdot \nu_{\partial\Omega} = \nabla\mu \cdot \nu_{\partial\Omega} = 0 \quad \text{on} \quad \partial\Omega.$$

3.1. **Matched asymptotic expansions.** In this section, we provide matched asymptotic expansions (see e.g. [18]) for the approximation of the above BCF–model by the diffuse-interface model (5)–(8). In order to achieve more rigorous results, one would have to apply techniques from [1].

In the following, we merge the asymptotic expansions in [5] and in [13] and apply the setup in [16]. The outer solution is an approximation to the solution on a terrace, the inner solution zooms in on a step. We make the following ansatz for the outer expansions:

$$\begin{aligned}\varrho_0 &= \varrho_{0,0} + O(\varepsilon),\\ \varrho_1 &= \varrho_{1,0} + O(\varepsilon),\\ \varphi &= \varphi_0 + O(\varepsilon),\\ \mu &= \mu_0 + O(\varepsilon).\end{aligned}$$

We consider a smeared-out step connecting a lower terrace where $\varphi \approx 0$ to an upper terrace where $\varphi \approx 1$. Let Γ denote the curve $\{\varphi = \frac{1}{2}\}$ with tangent τ. Let ν denote the normal of Γ (pointing from the upper to the lower terrace), κ its curvature, v its normal velocity. We further introduce the notation

$$\begin{aligned}s &:= \text{arc length along } \Gamma,\\ r &:= \text{signed distance to } \Gamma,\\ z &:= \varepsilon^{-1}r,\end{aligned}$$

where $r < 0$ in the upper terrace and $r > 0$ in the lower terrace. We transform

$$\begin{aligned}u_0(r,s,t) &= \varrho_0(x,y,t),\\ u_1(r,s,t) &= \varrho_1(x,y,t),\\ \phi(r,s,t) &= \varphi(x,y,t),\\ w(r,s,t) &= \mu(x,y,t)\end{aligned}$$

with corresponding outer expansions

$$\begin{aligned}u_0 &= u_{0,0} + O(\varepsilon),\\ u_1 &= u_{1,0} + O(\varepsilon),\\ \phi &= \phi_0 + O(\varepsilon),\\ w &= w_0 + O(\varepsilon),\end{aligned}$$

and we make the following transformation and ansatz for the inner expansions:

$$\begin{aligned} u_0(r,s,t) &= U_0(z,s,t) = U_{0,0}(z,s,t) + \varepsilon U_{0,1}(z,s,t) + O(\varepsilon^2),\\ u_1(r,s,t) &= U_1(z,s,t) = U_{1,0}(z,s,t) + \varepsilon U_{1,1}(z,s,t) + O(\varepsilon^2),\\ \phi(r,s,t) &= \Phi(z,s,t) = \Phi_0(z,s,t) + \varepsilon\,\Phi_1(z,s,t) + O(\varepsilon^2),\\ w(r,s,t) &= W(z,s,t) = W_0(z,s,t) + \varepsilon W_1(z,s,t) + \varepsilon^2 W_2(z,s,t) + O(\varepsilon^3). \end{aligned}$$

With this ansatz, we have

$$\partial_t\phi = -\varepsilon^{-1} v\partial_z\Phi + O(1), \tag{10}$$

$$\nabla\phi = \varepsilon^{-1}\partial_z\Phi\ \nu + (1+\varepsilon z\kappa)^{-1}\partial_s\Phi\ \tau, \tag{11}$$

$$\nabla\cdot j = \varepsilon^{-1}\partial_z(J\cdot\nu) + (1+\varepsilon z\kappa)^{-1}(\partial_s(J\cdot\tau) + \kappa J\cdot\nu), \tag{12}$$

where j denotes a vector field with $j(r,s,t) = J(z,s,t)$. Corresponding relations hold for U_0, U_1, W. Furthermore, we use matching conditions on inner and outer solutions

$$\lim_{z\to\pm\infty} U_{0,0} = \lim_{r\to\pm 0} u_{0,0}, \qquad \lim_{z\to\pm\infty}\partial_z U_{0,1} = \lim_{r\to\pm 0}\partial_r u_{0,0} = \lim_{r\to\pm 0}\partial_\nu\varrho_{0,0}, \tag{13}$$

$$\lim_{z\to\pm\infty} U_{1,0} = \lim_{r\to\pm 0} u_{1,0}, \qquad \lim_{z\to\pm\infty}\partial_z U_{1,1} = \lim_{r\to\pm 0}\partial_r u_{1,0} = \lim_{r\to\pm 0}\partial_\nu\varrho_{1,0}, \tag{14}$$

$$\lim_{z\to\pm\infty}\Phi_0 = \lim_{r\to\pm 0}\phi_0, \tag{15}$$

$$\lim_{z\to\pm\infty} W_0 = \lim_{r\to\pm 0} w_0. \tag{16}$$

3.1.1. *Outer Expansions.* The outer expansions to order $O(\varepsilon^{-1})$ yield in (8)

$$G'(\varphi_0) = 0 \quad\Longrightarrow\quad \varphi\in\{0,1\}, \tag{17}$$

from which we get in (5) and (6) to $O(\varepsilon^0)$

$$\partial_t(\varrho_{0,0}) = D\Delta\varrho_{0,0} + F - \tau_d^{-1}\varrho_{0,0} \quad\text{where}\quad \varphi_0 = 0, \tag{18}$$

$$\partial_t(\varrho_{1,0}) = D\Delta\varrho_{1,0} + F - \tau_d^{-1}\varrho_{1,0} \quad\text{where}\quad \varphi_0 = 1, \tag{19}$$

i.e. diffusion equations (1) for $\varrho_{0,0}$ and $\varrho_{1,0}$ on the lower and upper terrace, respectively.

3.1.2. *Inner Expansions.* The inner expansions in (8) lead to

$$\partial_z^2\Phi_0 - G'(\Phi_0) = 0 \tag{20}$$

to order $O(\varepsilon^{-1})$. In (7), leading orders $O(\varepsilon^{-3})$, $O(\varepsilon^{-2})$ yield

$$\partial_z W_0 = \partial_z W_1 = 0,$$

where the constant $W_0 = \kappa$ is the curvature of the step due to testing $O(\varepsilon^0)$ in (8) with $\partial_z\Phi_0$. From (15), we get to leading order $O(\varepsilon^{-2})$ in (5), (6)

$$\partial_z U_{0,0} = \partial_z U_{1,0} = 0,$$

and from (20) to order $O(\varepsilon^{-1})$

$$\begin{aligned} -v\partial_z((1-\Phi_0)U_{0,0}) &= D\partial_z((1-\Phi_0)\partial_z U_{0,1}) - B(\Phi_0)k_+(U_{0,0} - \varrho^*(1+\gamma\kappa)),\\ -v\partial_z(\Phi_0 U_{1,0}) &= D\partial_z(\Phi_0\partial_z U_{1,1}) - B(\Phi_0)k_-(U_{1,0} - \varrho^*(1+\gamma\kappa)), \end{aligned}$$

Integration leads to

$$\begin{aligned} -v\lim_{z\to\infty} U_{0,0} &= D\lim_{z\to\infty}\partial_z U_{0,1} - k_+(U_{0,0} - \varrho^*(1+\gamma\kappa)),\\ v\lim_{z\to-\infty} U_{1,0} &= -D\lim_{z\to-\infty}\partial_z U_{1,1} - k_-(U_{1,0} - \varrho^*(1+\gamma\kappa)), \end{aligned}$$

and hence, by matching conditions, $\varrho_{0,0}$ and $\varrho_{1,0}$ fulfil the boundary conditions (2) and (3), respectively. Going back to (7), we obtain in $O(\varepsilon^{-1})$

$$-v\partial_z\Phi_0 = \beta\partial_s^2\kappa + B(\Phi_0)(k_+(U_{0,0} - \varrho^*(1+\gamma\kappa)) + k_-(U_{1,0} - \varrho^*(1+\gamma\kappa))),$$

which gives by integration the evolution law

$$v = \beta\partial_s^2\kappa + k_+(\lim_{r\to+0} u_{0,0} - \varrho^*(1+\gamma\kappa)) + k_-(\lim_{r\to-0} u_{1,0} - \varrho^*(1+\gamma\kappa)),$$

which is equivalent to (4).

3.2. **Mass conservation and thermodynamic consistency.** Throughout this section, we assume $\tau_d^{-1} = 0$.

3.2.1. *Mass conservation.* In this section, we prove mass conservation of the diffuse-interface model. From (5)–(7), we obtain

$$\frac{\mathrm{d}}{\mathrm{d}t}\int_\Omega (\varphi + (1-\varphi)\varrho_0 + \varphi\varrho_1)\,\mathrm{d}x = F|\Omega|,$$

if we assume zero flux boundary conditions for μ, ϱ_0 and ϱ_1 on $\partial\Omega$. In other words, we obtain

$$M(t) = M(0) + F|\Omega|t,$$

if we define the total mass

$$\begin{aligned} M(t) :&= \int_\Omega (\varphi(x,t) + (1-\varphi(x,t))\varrho_0(x,t) + \varphi(x,t)\varrho_1(x,t))\,\mathrm{d}x \\ &\approx |\Omega_1(t)| + \int_{\Omega_0(t)} \varrho_0(x,t)\,\mathrm{d}x + \int_{\Omega_1(t)} \varrho_1(x,t)\,\mathrm{d}x \end{aligned}$$

in the diffuse-interface setting.

3.2.2. *Thermodynamic consistency.* Here, we prove that the diffuse-interface approximation

$$\mathcal{E}(\varphi) := \int_\Omega \Big(\frac{\varepsilon}{2}|\nabla\varphi|^2 + \varepsilon^{-1}G(\varphi)\Big)\,\mathrm{d}x$$

of the total length of the steps satisfies

$$\frac{\mathrm{d}}{\mathrm{d}t}\mathcal{E} \le 0, \tag{21}$$

if we assume vanishing deposition flux $F = 0$ and quasi-stationary versions of (5), (6) as well as zero flux boundary conditions for μ, ϱ_0 and ϱ_1 on $\partial\Omega$. For the proof of (21), we observe

$$\begin{aligned} \frac{\mathrm{d}}{\mathrm{d}t}\mathcal{E} &= \int_\Omega \mu\partial_t\varphi\,\mathrm{d}x \le \int_\Omega \mu\varepsilon^{-1}B(\varphi)(k_+(\varrho_0 - \varrho^*(1+\gamma\mu)) + k_-(\varrho_1 - \varrho^*(1+\gamma\mu)))\,\mathrm{d}x \\ &= \int_\Omega \frac{\varrho_0-\varrho^*}{\varrho^*\gamma}\varepsilon^{-1}B(\varphi)k_+(\varrho_0 - \varrho^*(1+\gamma\mu))\,\mathrm{d}x + \int_\Omega \frac{\varrho_1-\varrho^*}{\varrho^*\gamma}\varepsilon^{-1}B(\varphi)k_-(\varrho_1 - \varrho^*(1+\gamma\mu))\,\mathrm{d}x \\ &\quad + \int_\Omega \Big(\mu - \frac{\varrho_0-\varrho^*}{\varrho^*\gamma}\Big)\varepsilon^{-1}B(\varphi)k_+(\varrho_0 - \varrho^*(1+\gamma\mu))\,\mathrm{d}x \\ &\quad + \int_\Omega \Big(\mu - \frac{\varrho_1-\varrho^*}{\varrho^*\gamma}\Big)\varepsilon^{-1}B(\varphi)k_+(\varrho_1 - \varrho^*(1+\gamma\mu))\,\mathrm{d}x. \end{aligned}$$

Since the two last integrals are non-positive, we obtain by (5) and (6)

$$\frac{\mathrm{d}}{\mathrm{d}t}\mathcal{E} \le \int_\Omega \frac{\varrho_0-\varrho^*}{\varrho^*\gamma}D\nabla\cdot((1-\varphi)\nabla\varrho_0)\,\mathrm{d}x + \int_\Omega \frac{\varrho_1-\varrho^*}{\varrho^*\gamma}D\nabla\cdot(\varphi\nabla\varrho_1)\,\mathrm{d}x \le 0$$

with integration by parts and the additional assumption $\varphi \in [0,1]$.

3.3. **More than two terraces.** In order to extend the diffuse-interface model (5)–(8) to a situation with more than two terraces, we have to periodically extend the functions G, B, $H_0 = H_0(\varphi) = 1-\varphi$, $H_1 = H_1(\varphi) = \varphi$, $\varphi \in [0,1]$, to be more precise, we one-periodically extend G and B, whereas H_0 and H_1 are two-periodically extended after the extension

$$\begin{aligned} H_0(\varphi) &= -1+\varphi \quad \text{for} \quad \varphi \in (1,2], \\ H_1(\varphi) &= 2-\varphi \quad \text{for} \quad \varphi \in (1,2]. \end{aligned}$$

Furthermore, we introduce

$$B_{0/1}(\varphi) := B(\varphi) \begin{cases} k_\pm & \text{for } \varphi \in [0,1), \\ k_\mp & \text{for } \varphi \in [1,2) \end{cases}$$

and extend $B_{0/1}$ two-periodically in order to decide, if there is a step up or down. The resulting system then reads

$$\begin{aligned} \partial_t(H_0(\varphi)\varrho_0) &= D\nabla\cdot(H_0(\varphi)\nabla\varrho_0) + H_0(\varphi)F - H_0(\varphi)\tau_d^{-1}\varrho_0 \\ &\quad - \varepsilon^{-1}B_0(\varphi)(\varrho_0 - \varrho^*(1+\gamma\mu)), \end{aligned} \tag{22}$$

$$\begin{aligned} \partial_t(H_1(\varphi)\varrho_1) &= D\nabla\cdot(H_1(\varphi)\nabla\varrho_1) + H_1(\varphi)F - H_1(\varphi)\tau_d^{-1}\varrho_0 \\ &\quad - \varepsilon^{-1}B_1(\varphi)(\varrho_1 - \varrho^*(1+\gamma\mu)), \end{aligned} \tag{23}$$

$$\begin{aligned} \partial_t\varphi &= \varepsilon^{-1}\beta\nabla\cdot(B(\varphi)\nabla\mu) + \varepsilon^{-1}B_0(\varphi)(\varrho_0 - \varrho^*(1+\gamma\mu)) \\ &\quad + \varepsilon^{-1}B_1(\varphi)(\varrho_1 - \varrho^*(1+\gamma\mu)), \end{aligned} \tag{24}$$

$$\mu = -\varepsilon\Delta\varphi + \varepsilon^{-1}G'(\varphi). \tag{25}$$

4. Numerical results

In this section, we present numerical results obtained by a FEM discretisation (linear elements) of system (22)–(25). We use a straight forward discretisation, where we linearise all nonlinear terms and solve as system for the discrete counterpart of (22)–(25). We apply an adaptive strategy in space with an L^2–like error indicator based on a jump residual for φ and a simple time adaptive approach, where the m-th time step Δt_m is inversely proportional to the maximum of the discrete time derivative of the phase-field variable (see e.g. [21] for more details). The algorithm is implemented in the FEM toolbox AMDiS [24]. The resulting linear system of equations is solved by a direct solver (UMFPACK, [6]).

In sections 4.1–4.3 we study the quasi-stationary case, where in the BCF–model, (1) is assumed stationary with zero left hand side. In addition, mass conservation yields that the convective terms $\varrho_i v$ in (2), (3) have to be neglected. This corresponds to zero left hand sides in (22)–(23).

Moreover, we regularise all second order terms in equations (22)–(25) by adding a small positive parameter $\delta = \delta(\varepsilon) \ll \varepsilon$ to the functions H_0, H_1 and B, respectively in all second order differential operators. In all simulations, we have chosen the value $\delta = 10^{-5}$. Furthermore, we replace μ in (25) by $g(\varphi)\mu$ with $g(\varphi) := 30\varphi^2(1-\varphi)^2$ in order to stabilise the numerical scheme. Neither of both regularisations has an influence on the results of the asymptotic analysis in section 3.1 [21].

4.1. **1d examples.** First, we reproduce the results of the asymptotic analysis in one dimension and compare discrete adatom densities with analytic solutions. Here, the analytic adatom concentration in the quasi-stationary BCF–model is

$$c(x) = \begin{cases} c_0(x) = -\frac{F}{2D}\left(x^2 - R^2\right) + \frac{F}{D}(x-R) + \frac{F}{k_+}(1-R) & \text{for} \quad x > R, \\ c_1(x) = -\frac{F}{2D}\left(x^2 - R^2\right) - \frac{F}{D}(x-R) + \frac{F}{k_-}(1+R) & \text{for} \quad x < R, \end{cases}$$

where the interface R is given by $R(t) = 2Ft$ and $c_i := \varrho_i - \varrho^*$, $i = 0, 1$, denote excess adatom densities. For the diffuse-interface model, we have used the initial condition

$$\varphi(x,0) = \frac{1}{2}\left(1 - \tanh\left(\frac{3x}{\varepsilon}\right)\right),$$

constant time steps of length $\Delta t = 2 \cdot 10^{-4}$ and uniform meshes. Moreover, we have chosen the following set of academic parameters

$$k_+ = 10; \quad k_- = 1; \quad \varrho^* = 0.1; \quad \gamma = 10; \quad D = 10; \quad F = 0.1; \quad \tau_d^{-1} = 0; \quad \beta = 0. \tag{26}$$

Let c_0^h, c_1^h and φ^h denote the discrete excess adatom concentrations and phase-field function, respectively. In Fig. 2, we present the convergence of the discrete excess adatom densities towards the analytic solution for decreasing ε, where on the left, one can see complete plots of the discrete excess densities c_0^h, c_1^h, whereas on the right, only the relevant parts of the plots of c_0^h (for $\varphi^h \leq 0.5$) and c_1^h (for $\varphi^h \geq 0.5$) are shown. The remaining parts of c_0^h, c_1^h are meaningless.

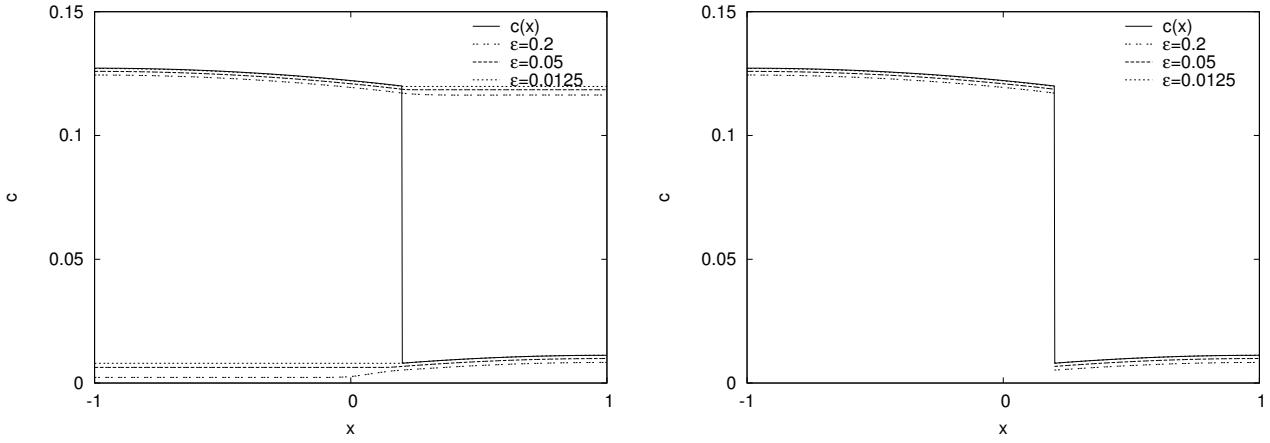

FIGURE 2. Left: Discrete adatom excess concentrations c_0^h, c_1^h for $\varepsilon = 0.2$, $\varepsilon = 0.05$ and $\varepsilon = 0.0125$ and analytic excess concentration c. Right: Corresponding plots, where only relevant parts of c_0^h (where $\varphi^h \leq 0.5$), c_1^h (where $\varphi^h \geq 0.5$) are shown.

In addition, we compare in Fig. 3 the above results with ones obtained by the diffuse-interface approximation in [16] (see [20] for the discretisation) for the same $\varepsilon = 0.025$. One can see that the approximation by (22)–(25) is slightly better.

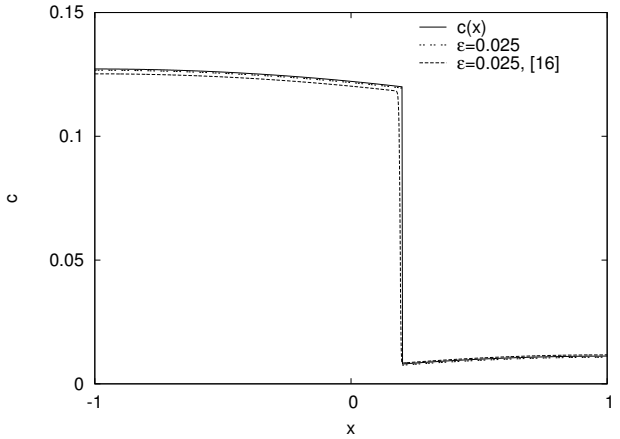

FIGURE 3. Discrete adatom excess concentrations c_0^h, c_1^h for $\varepsilon = 0.025$ and discrete excess adatom concentration obtained by the diffuse-interface model in [16] with $\varepsilon = 0.025$ and analytic excess concentration c.

4.2. **2d circular island.** In the two dimensional case, we consider a circular shaped domain $\Omega := B_{R_\infty}(0)$ with $R_\infty = 5$ and the time interval $[0, t_\infty]$ with $t_\infty := \frac{1-(R_0/R_\infty)^2}{F}$. The initial circular shaped epitaxial island $\Gamma(t=0) = \partial B_{R_0}(0)$ with $R_0 = 2$ is introduced.

The quasi-stationary rotationally symmetric analytic adatom density in this situation reads (see [12])

$$c(r) = \begin{cases} c_0(r) & = \frac{F}{4D}\left(R^2 - r^2\right) + \frac{FR_\infty^2}{2D}\log\left(\frac{r}{R}\right) + \frac{\varrho^*\gamma}{R} + \frac{F}{2k_+}\left(\frac{R_\infty^2}{R} - R\right) \quad \text{for} \quad r > R, \\ c_1(r) & = \frac{F}{4D}\left(R^2 - r^2\right) + \frac{\varrho^*\gamma}{R} + \frac{FR}{2k_-} \quad \text{for} \quad r < R \end{cases}$$

with $r := |x|$ and $\Gamma(t) = \partial B_{R(t)}(0)$, where

$$R(t) = \sqrt{R_0^2 + FR_\infty^2 t}. \tag{27}$$

By (27) one obtains the relation $R(t_\infty) = R_\infty$. For the diffuse-interface approximation, we choose the initial condition

$$\varphi(x,0) = \frac{1}{2}\left(1 - \tanh\left(\frac{3(|x| - R_0)}{\varepsilon}\right)\right) \tag{28}$$

corresponding to the one of the sharp-interface model. Furthermore, we use the same parameters as in the one dimensional case, except $\gamma = 1$ instead of $\gamma = 10$. Moreover, we choose the constant time steps $\Delta t = 2 \cdot 10^{-4}$, and we apply local mesh refinement in space.

Then we first look at the adatom concentrations c_i^h, $i = 0, 1$ at time $t = 0.5$ for $\varepsilon = 0.2, 0.1, 0.05$ in Fig. 4 (left), where one can see the approximation of the analytic adatom concentration c for decreasing ε.

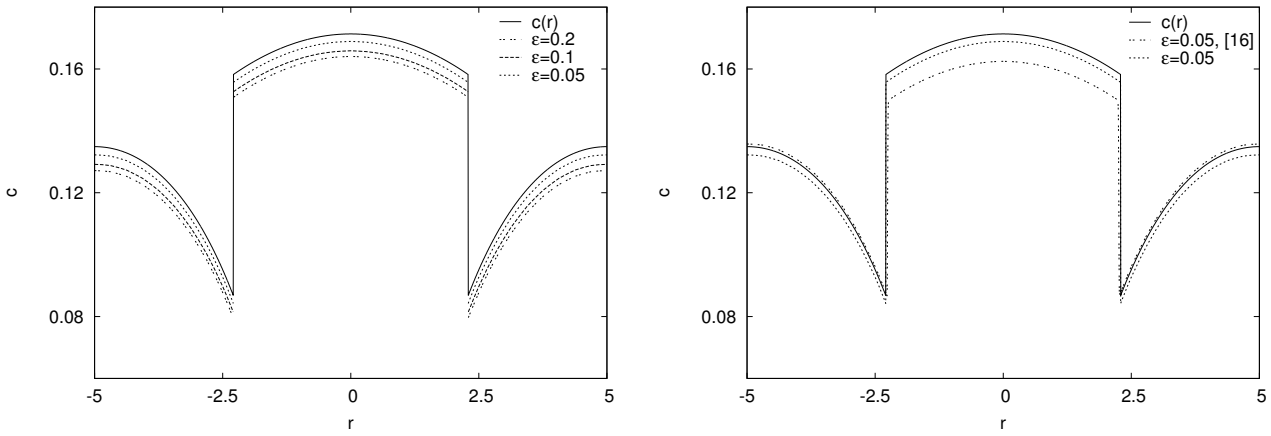

FIGURE 4. Left: Discrete adatom excess concentrations c_0^h, c_1^h for $\varepsilon = 0.2$, $\varepsilon = 0.1$ and $\varepsilon = 0.025$ and analytic excess concentration c, where only relevant parts of c_0^h (where $\varphi^h \leq 0.5$), c_1^h (where $\varphi^h \geq 0.5$) are shown. Right: Discrete adatom excess concentrations c_0^h, c_1^h for $\varepsilon = 0.05$ and discrete excess adatom concentration obtained by the diffuse-interface model in [16] and analytic excess concentration c.

Moreover, we compare the numerical results obtained by the discretisation of (22)–(25) with the ones obtained by the model in [16], where the approximation by the former is better on the upper terrace, but worse on the lower terrace. An advantage of the former approach is that in contrast to latter one, the steps are not "behind" the analytic solution as it is reported in [17, 20]. However, this phenomenon is more relevant for increased deposition flux. In [9], this difficulty has been circumvented by a modification of the multiwell potential as well as by adding the first order outer solution of the asymptotic analysis to the initial phase-field function.

4.3. **comparison with stability analysis.** In this section, we follow the stability analysis for a single circular island presented in [12] and consider the circular domain $\Omega := B_{R_\infty}(0)$, the boundary of a circular island ∂B_{R_0} and a perturbed interface $\tilde{\Gamma} := \partial B_{\tilde{R}}(0)$ with a perturbation $\tilde{R} := R_0 + A_0 \cos l\theta$ of the radius R_0 with amplitude A_0 and wavenumber l. For the growth rate $\omega = \omega(l,t)$, one obtains (see [12])

$$\begin{aligned}\partial_t \omega(l,t) = &- \frac{F}{2\mathcal{A}} - \frac{\beta(l^4-l^2)}{R_\infty^4 \mathcal{A}^2} - \frac{Dl\left(\frac{F}{2} + \frac{k_- F R_\infty \mathcal{A}^{1/2}}{2D} + \frac{k_- \varrho^* \gamma (l^2-1)}{R_\infty^2 \mathcal{A}}\right)}{Dl + k_- R_\infty \mathcal{A}^{1/2}} \\ &+ \frac{Dl\left(1-\mathcal{A}^l\right)\left(\frac{F}{2}\left(1+\frac{1}{\mathcal{A}}\right) + \frac{k_+ F R_\infty \mathcal{A}^{1/2}}{2D}\left(\frac{1}{\mathcal{A}}-1\right) - \frac{k_+ \varrho^* \gamma (l^2-1)}{R_\infty^2 \mathcal{A}}\right)}{k_+ R_\infty \mathcal{A}^{1/2}\left(\mathcal{A}^l+1\right) + Dl\left(1-\mathcal{A}^l\right)},\end{aligned} \tag{29}$$

where $\mathcal{A} = \mathcal{A}(t) := R^2(t)/R_\infty^2$ denotes the rescaled area of the unperturbed island (see (27)). Then for moderate values of $k_\pm$ and γ and for F/D sufficiently large, one can expect unstable behaviour of sufficiently small islands [12]. Here, we choose

$$k_+ = 10; \quad k_- = 1; \quad F = 1; \quad D = 1; \quad \varrho^* = 0.1; \quad \gamma = 0.5; \quad \beta = 0.$$

In addition, we have used $\varepsilon = 0.025$, $R_\infty = 5$ and the initial condition

$$\varphi(x,0) = \frac{1}{2}\left(1 - \tanh\left(\frac{3(|x| - \tilde{R})}{\varepsilon}\right)\right)$$

with $R_0 = 1$, $A_0 = 0.005$ and an unstable wavenumber $l = 9$. This leads to the numerical results of the diffuse-interface approximation in Fig. 5 (right) showing the level sets $\{\varphi^h = 1/2\}$ at different times, where we have used time steps $\Delta t = 10^{-4}$ and an adaptive grid for the spatial discretisation.

Thereby, one observes an unstable behaviour at the beginning and a stabilisation starting, when the island is sufficiently large, which corresponds to the fact that $\partial_t \omega(l,t) < 0$ holds for any wavenumber l and for islands satisfying

$$\mathcal{A}(t) \geq k_+/(k_+ + k_-)$$

as shown in [12]. In Fig. 5 (left), we compare the growth rate numerically obtained by a diffuse-interface simulation with the numerical integration (with Maple) of the dispersion relation (29).

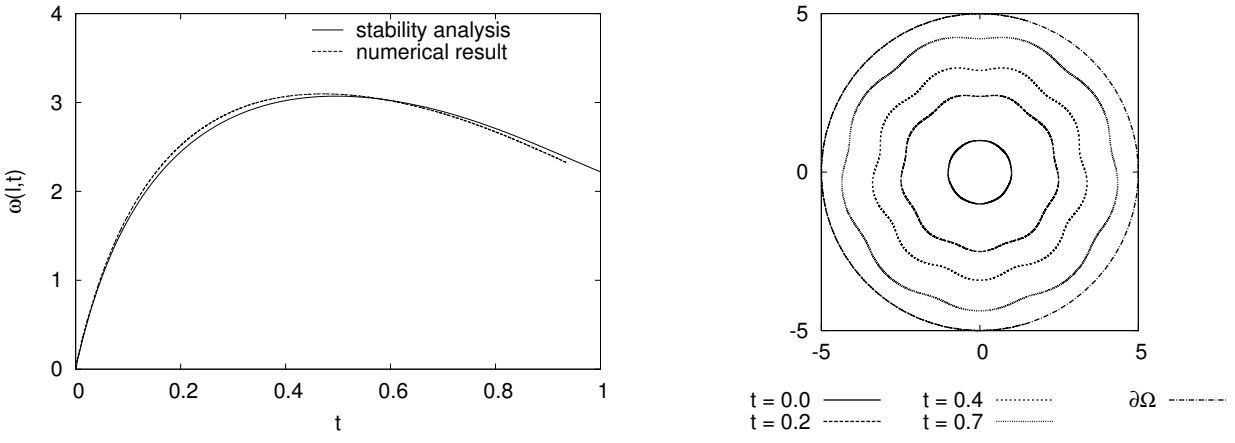

FIGURE 5. Left: Comparison of theoretical and numerical growth rate. Right: Unstable growth of perturbed circular island, level lines $\{\varphi^h = \frac{1}{2}\}$ at different times.

The above instability vanishes, if we include edge diffusion with $\beta = 1$. This is displayed in the plot of the analytic growth rate in Fig. 6 (left) and in the level lines obtained by the numerical treatment of (22)–(25) in Fig. 6 (right).

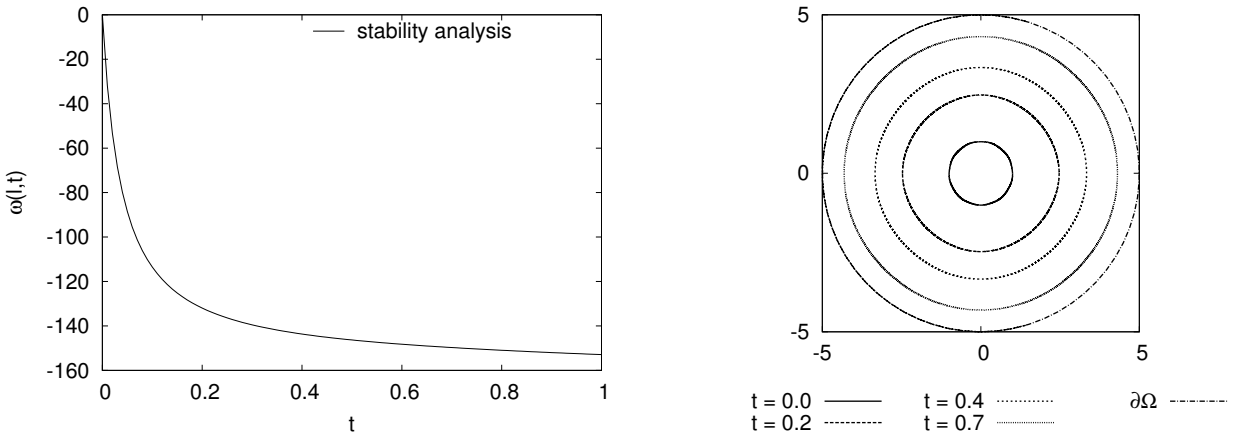

FIGURE 6. Left: Theoretical growth rate for $\beta = 1$. Right: Stable growth of perturbed circular island for $\beta = 1$, level lines $\{\varphi^h = \frac{1}{2}\}$ at different times.

4.4. **More than two terraces.** In this section and in contrast to the previous numerical examples, we present numerical results for the diffuse-interface approximation (5)–(8) with non-vanishing left hand sides in (5)–(6). Here, we have used the domain $\Omega = (-10, 10)^2$, adaptivity in time and space and $\varepsilon = 0.1$. Moreover, we have applied the parameters from section 4.2, but in order to investigate the influence of edge diffusion, we have varied the parameter β. In Fig. 7, one can see numerical results (contour plots of the discrete phase-field function φ^h), where we have started our simulations with two islands of height one and one island of height two. Furthermore, we have used initial adatom concentrations $\varrho_i(x, 0) \equiv 0.25$, $i = 0, 1$. The upper row shows the phase field function at different times for moderate edge diffusion parameter $\beta = 1$. The evolution does not include any coalescence of islands, whereas for increased edge diffusion parameter $\beta = 10$, circular islands are more stable and we see in the lower row the coalescence of two islands, which further illustrates the influence of edge diffusion on the evolution.

REFERENCES

[1] N.D. Alikakos, P.W. Bates, and X. Chen. The convergence of solutions of the Cahn-Hilliard equation to the solution of the Hele-Shaw model. *Arch. Rational Mech. Anal.*, 128(2):165–205, 1994.

[2] G.S. Bales and A. Zangwill. Morphological instability of a terrace edge during step-flow growth. *Phys. Rev. B*, 41(9):5500–5508, 1990.

[3] E. Bänsch, F. Haußer, O. Lakkis, B. Li, and A. Voigt. Finite element method for epitaxial growth with attachment-detachment kinetics. *J. Comput. Phys.*, 194(2):409–434, 2004.

[4] W.K. Burton, N. Cabrera, and F.C. Frank. The growth of crystals and the equilibrium of their surfaces. *Phil. Trans. Roy. Soc. London Ser. A*, 243(866):299–358, 1951.

[5] J.W. Cahn, C.M. Elliott, and A. Novick-Cohen. The Cahn-Hilliard equation with a concentration-dependent mobility: Motion by minus the Laplacian of the mean curvature. *Euro. J. Appl. Math.*, 7:287–301, 1996.

[6] T.A. Davis. Algorithm 832: UMFPACK V4.3—an unsymmetric-pattern multifrontal method. *ACM Trans. Math. Software*, 30(2):196–199, 2004.

[7] G. Ehrlich and F.G. Hudda. Atomic view of surface diffusion: tungsten on tungsten. *J. Chem. Phys.*, 44:1036–1099, 1966.

[8] Z. Hu, S. Li, and J.S. Lowengrub. Morphological stability analysis of the epitaxial growth of a circular island: application to nanoscale shape control. *Phys. D*, 233(2):151–166, 2007.

[9] Z. Hu, J.S. Lowengrub, S.M. Wise, and A. Voigt. Phase-field modeling of epitaxial growth: Applications to step trains and island dynamics. *Phys. D*, 241:77–94, 2012.

[10] A. Karma and M. Plapp. Spiral surface growth without desorption. *Phys. Rev. Lett.*, 81:4444–4447, 1998.

[11] J. Krug. Introduction to step dynamics and step instabilities. In A. Voigt, editor, *Multiscale modeling of epitaxial growth*, volume 149 of *ISNM*, pages 59–95. Birkhäuser, Basel, 2005.

[12] B. Li, A. Rätz, and A. Voigt. Stability of a circular epitaxial island. *Phys. D*, 198:231–247, 2004.

[13] X. Li, J. Lowengrub, A. Rätz, and A. Voigt. Solving PDEs in complex geometries: a diffuse domain approach. *Commun. Math. Sci.*, 7(1):81–107, 2009.

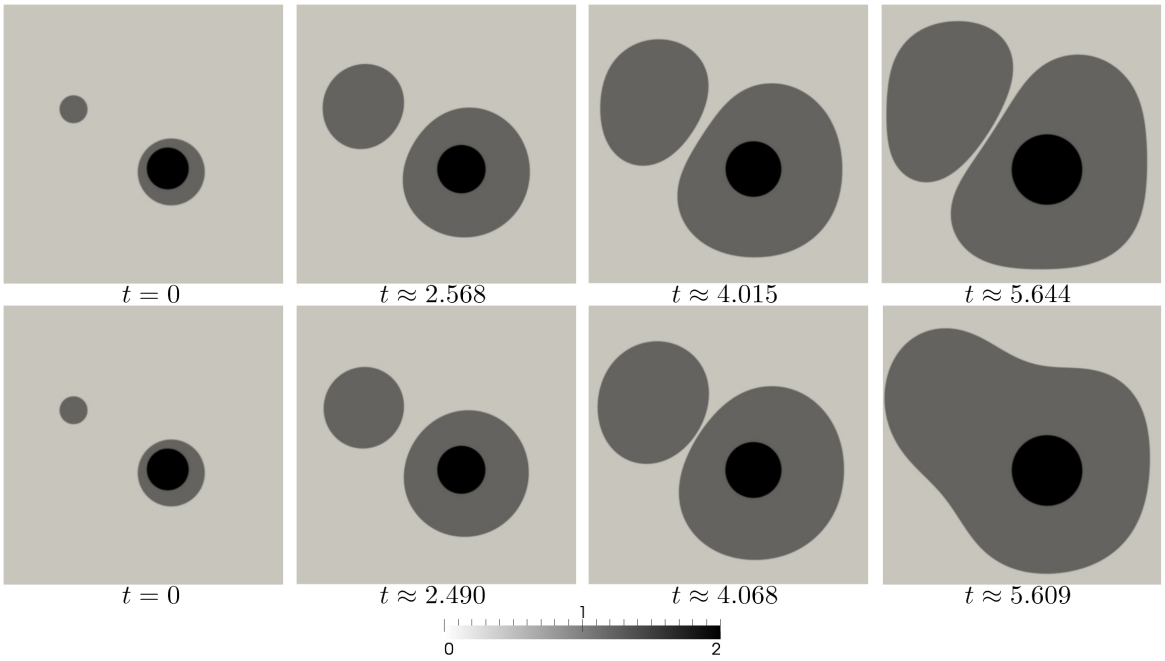

FIGURE 7. Three islands of different heights at different times. Upper row: moderate edge diffusion ($\beta = 1$), discrete phase-field function φ^h at $t = 0$, $t \approx 2.568$, $t \approx 4.015$, $t \approx 5.644$. Lower row: enhanced edge diffusion ($\beta = 10$), discrete phase-field function φ^h at $t = 0$, $t \approx 2.490$, $t \approx 4.068$, $t \approx 5.609$.

[14] F. Liu and H. Metiu. Stability and kinetics of step motion on crystal surfaces. *Phys. Rev. E*, 49:2601–2616, 1994.
[15] T. Michely and J. Krug. *Islands, Mounds and Atoms*. Springer, 2004. Patterns and Processes in Crystal Growth Far from Equilibrium.
[16] F. Otto, P. Penzler, A. Rätz, T. Rump, and A. Voigt. A diffuse-interface approximation for step flow in epitaxial growth. *Nonlinearity*, 17:477 – 491, 2004.
[17] F. Otto, P. Penzler, and T. Rump. Discretisation and Numerical tests of a Diffuse-Interface Model with Ehrlich-Schwoebel Barrier. In A. Voigt, editor, *Multiscale modeling of epitaxial growth*, volume 149 of *ISNM*, pages 127–159. Birkhäuser, Basel, 2005.
[18] R. Pego. Front migration in the nonlinear Cahn-Hilliard equation. *Proc. Roy. Soc. London Ser. A*, 422:261–278, 1989.
[19] O. Pierre-Louis. Phase field models for step flow. *Phys. Rev. E*, 68(2):021604, 2003.
[20] A. Rätz. *Modelling and numerical treatment of diffuse-interface models with applications in epitaxial growth.* PhD thesis, Bonner Mathematische Schriften 385. Bonn: Univ. Bonn, Mathematisches Institut (Dissertation). vi, 94 p. , 2007.
[21] A. Rätz, A. Ribalta, and A. Voigt. Surface evolution of elastically stressed films under deposition by a diffuse interface model. *J. Comput. Phys.*, 214(1):187–208, 2006.
[22] R.L. Schwoebel. Step motion on crystal surfaces II. *J. Appl. Phys.*, 40:614–618, 1969.
[23] R.L. Schwoebel and E.J. Shipsey. Step motion on crystal surfaces. *J. Appl. Phys.*, 37:3682–3686, 1966.
[24] S. Vey and A. Voigt. AMDiS — adaptive multidimensional simulations. *Comput. Visual. Sci.*, 10:57–67, 2007.
[25] Y.-M. Yu, R. Backofen, and A. Voigt. A phase-field simulation of stripe arrays on metal bcc(100) surfaces. *Phys. Rev. E*, 77:051605, 2008.
[26] Y.-M. Yu and A. Voigt. Directed self-organization of trench templates for nanowire growth. *Appl. Phys. Lett.*, 94:043108, 2009.

Preprints ab 2009/17

2012-03 **Andreas Rätz**
A new diffuse-interface model for step flow in epitaxial growth

2012-02 **Andreas Rätz and Ben Schweizer**
Hysteresis models and gravity fingering in porous media

2012-01 **Wilfried Hazod**
Intrinsic topologies on H-contraction groups with applications to semistability

2011-14 **Guy Bouchitté and Ben Schweizer**
Plasmonic waves allow perfect transmission through sub-wavelength metallic gratings

2011-13 **Waldemar Grundmann**
Moment functions and Central Limit Theorem for Jacobi hypergroups on $[0, \infty[$

2011-12 **J. Koch, A. Rätz, and B. Schweizer**
Two-phase flow equations with a dynamic capillary pressure

2011-11 **Michael Voit**
Central limit theorems for hyperbolic spaces and Jacobi processes on $[0, \infty[$

2011-10 **Ben Schweizer**
The Richards equation with hysteresis and degenerate capillary pressure

2011-09 **Andreas Rätz and Matthias Röger**
Turing instabilities in a mathematical model for signaling networks

2011-08 **Matthias Röger and Reiner Schätzle**
Control of the isoperimetric deficit by the Willmore deficit

2011-07 **Frank Klinker**
Generalized duality for k-forms

2011-06 **Sebastian Aland, Andreas Rätz, Matthias Röger, and Axel Voigt**
Buckling instability of viral capsides - a continuum approach

2011-05 **Wilfried Hazod**
The concentration function problem for locally compact groups revisited: Non-dissipating space-time random walks, τ-decomposable laws and their continuous time analogues

2011-04 **Wilfried Hazod, Katrin Kosfeld**
Multiple decomposability of probabilities on contractible locally compact groups

2011-03 **Alexandra Monzner* and Frol Zapolsky†**
A comparison of symplectic homogenization and Calabi quasi-states

2011-02 **Stefan Jäschke, Karl Friedrich Siburg and Pavel A. Stoimenov**
Modelling dependence of extreme events in energy markets using tail copulas

2011-01 **Ben Schweizer and Marco Veneroni**
The needle problem approach to non-periodic homogenization

2010-16 **Sebastian Engelke and Jeannette H.C. Woerner**
A unifying approach to fractional Lévy processes

2010-15 **Alexander Schnurr and Jeannette H.C. Woerner**
Well-balanced Lévy Driven Ornstein-Uhlenbeck Processes

2010-14 **Lorenz J. Schwachhöfer**
On the Solvability of the Transvection group of Extrinsic
Symplectic Symmetric Spaces

2010-13 **Marco Veneroni**
Stochastic homogenization of subdifferential inclusions via scale integration

2010-12 **Agnes Lamacz, Andreas Rätz, and Ben Schweizer**
A well-posed hysteresis model for flows in porous media and
applications to fingering effects

2010-11 **Luca Lussardi and Annibale Magni**
Γ-limits of convolution functionals

2010-10 **Patrick W. Dondl, Luca Mugnai, and Matthias Röger**
Confined elastic curves

2010-09 **Matthias Röger and Hendrik Weber**
Tightness for a stochastic Allen–Cahn equation

2010-08 **Michael Voit**
Multidimensional Heisenberg convolutions and product formulas
for multivariate Laguerre polynomials

2010-07 **Ben Schweizer**
Instability of gravity wetting fronts for Richards equations with hysteresis

2010-06 **Lorenz J. Schwachhöfer**
Holonomy Groups and Algebras

2010-05 **Agnes Lamacz**
Dispersive effective models for waves in heterogeneous media

2010-04 **Ben Schweizer and Marco Veneroni**
Periodic homogenization of Prandtl-Reuss plasticity equations in arbitrary dimension

2010-03 **Holger Dette and Karl Friedrich Siburg and Pavel A. Stoimenov**
A copula-based nonparametric measure of regression dependence

2010-02 **René L. Schilling and Alexander Schnurr**
The Symbol Associated with the Solution of a Stochastic Differential Equation

2010-01 **Henryk Zähle**
Rates of almost sure convergence of plug-in estimates for distortion risk measures